KSCE Journal of Civil Engineering (2021) 25(2):386-397
DOI 10.1007/s12205-020-2131-6

pISSN 1226-7988, eISSN 1976-3808
www.springer.com/12205

Geotechnical Engineering

# Examination of Interface Asperity and Particle Shape on the Mechanical Behavior of Soil-Structure Interfaces Using 3D Printed Models

**Xin Kang**[a], **Hang Lei**[a], **and Renpeng Chen**[a]

[a]*Dept. of Geotechnical Engineering, College of Civil Engineering, Hunan University, Changsha 410082, China*

**ARTICLE HISTORY**

Received 24 November 2019
Accepted 16 September 2020
Published Online 4 December 2020

**KEYWORDS**

Soil-structure interface
Interface topography
3D printing
Direct shear test
Particle characteristics

**ABSTRACT**

The influence of surface topography on the mechanical behavior of soil-structure interfaces over a range of particle sizes and shapes is systematically investigated in this research. 3D printed interfaces with different topographies and uniformly graded 3D printed soil particles and two types of natural sands (Ottawa sand 20/30 and Dolomite sand #1, #2 and #3) were employed and tested. Laboratory investigations showed that the shear strength and volume change responses of the 3D printed interfaces are positively influenced with the increase of the inclination of asperities. The proposed wedge friction model successfully explained the distinct mechanical behaviors of soil-structure interfaces under shearing. A "turning point" was found for the interface shear resistance with the increase of the inclination of asperities. When the surface topography produces passive resistance to the soil, the change of the surface topography has little effect on the interface mechanical behavior. The findings from this research will provide insights for soil-structure interface design and discrete element method (DEM) simulations in considering the mechanical behavior of soil-structure interfaces.

## 1. Introduction

The interfacial friction performance between soils and structures controls the capacity of many infrastructures and the efficiency of construction processes, which is shown in deep foundations, tunneling and transport processes. It is meaningful to study the behavior of soil-structure interfaces for the structural design of various geo-infrastructures (Jardine et al., 1993; Won and Kim, 2007; Kang et al., 2012; Portelinha et al., 2014; Tehrani et al., 2016). To this propose, many laboratory tests and numerical simulations have been introduced which indicate the interface roughness plays an important role in governing the soil-structure interactions (Milligan and Tei, 1998; Frost and DeJong, 2005; DeJong et al., 2017; Martinez and Frost, 2017; Jing et al., 2017; Martinez and Palumbo, 2018). There are many parameters to quantitatively characterize the interface roughness. For example, the most commonly used and applicable one is the relative roughness ($R_n$) proposed by Uesugi and Kishida (1986a). When the mean particle size ($D_{50}$) is used as the gauge length, the ratio of the measured maximum height of asperity ($R_{max}$) to $D_{50}$ is referred to as $R_n$ of the interface. Hu and Pu (2004) proposed the concept of critical relative roughness ($R_{cr}$), and based on $R_{cr}$, the interface was categorized into two types: smooth and rough, according to the shear failure mode. Liu et al. (2009) studied the mechanical behavior of soil-geogrid interface and found that bearing resistance provided by transverse ribs has an effect on interface shear resistance. The contribution of resistance was verified to be related to $D_{50}$.

Several researchers suggest that the surface topography and stress path have positive effects in enhancing the transfer of interface shear load (Kang and Kang, 2015; Kang et al., 2016). As the surface topography size increases, not only the friction between soil particles and material surface, but also the passive resistance from surface topography has an effect on mechanical behavior of soil-structure interfaces (Mitchell and Villet, 1987; Tang et al., 2010; Martinez and Frost, 2017). As the engineering structure becomes larger and more important, the soil-structure interface study should not only consider the results of the friction response, the difference of interface mechanical behavior caused by the surface topography is also the key point to the interface design. Soil or material surface topography has great effects on the mechanical behavior of interface (Michalowski and Čermák, 2002; Wang et al., 2007; Farhadi and Lashkari, 2017). However, the quantitative characterization of surface topography related to

**CORRESPONDENCE** Xin Kang kangxin@hnu.edu.cn Dept. of Geotechnical Engineering, College of Civil Engineering, Hunan University, Changsha 410082, China

the direction is not widely practiced even if analytical methods exist for determining the shear behaviors. Researching the mechanism of differences in interface mechanical behavior caused by different directions of shear force plays a guiding role in future interface design or discrete element method (DEM) models.

Direct shear tests are often conducted to investigate the interactions between soil and structure interfaces but most researchers focused only on the effects of material surface topography (Rourke et al., 1990; Subba Rao et al., 1998; Dove and Jarrett, 2002). Experimental and theoretical studies have revealed that not only surface topography performance, but also several other factors, including soil particle characteristics (size and shape), soil relative density and the normal stress level have great effects on interface behavior by influencing the interaction between granular material and contact surface (Rourke et al., 1990; Hryciw and Irsyam, 1993; Lings and Dietz, 2005; Tiwari et al., 2010; Yavari et al., 2016; Afzali-Nejad et al., 2017). $D_{50}$ and shape parameters are widely used in describing the particle characteristics. However, the methods of defining the shape of a particle are mostly very simple and unscientific (Uesugi and Kishada, 1986b; Yudhbir and Abedinzadeh, 1991; Sukumaran and Ashmawy, 2001). Compared with two-dimensional projection parameter, shape information of a particle is holistically exhibited in three-dimensional. Therefore, a new three-dimensional shape parameter called surface area-to-volume ($A/V$) ratio is defined on this basis to represent aggregate's topography. $A/V$ is also found to have close relationship with the mechanical behavior (Lee et al., 2019; Su et al., 2020).

In the past decades, the 3D printing, which regarded as a new field, is experiencing rapid development with new technologies and materials being introduced at an impressive rate. The 3D printing has stimulated interest into possible applications in the field of geotechnics with plenty of laboratory tests conducted in recent years (Hanaor et al., 2016; Adamidis et al., 2020; Su et al., 2020). 3D printing has brought unprecedented convenience to the design of complex topography. In particular, 3D printing provides a unique opportunity to create granular materials with independent control of particle size and shape; therefore, the 3D printing not only offers better prediction of the mechanical behavior of soil-structure interface on a description of particle or material surface asperity shape, but also greatly advances the state-of-art in the fields of soil mechanics, deep foundation engineering, landfill slopes, and material transport processes, etc.

This paper investigated the effects of inclination of asperity, particle size and shape on the mechanical behavior of soil-structure interfaces. To this purpose, structure interfaces manufactured by 3D printing are divided into six types in accordance with interface shape factor ($\lambda$) (see section 3 for more details) related to the direction of applied force. Ottawa sand 20/30, three types of Dolomite sand with different $D_{50}$ and four types of 3D printed plastic particles with different particle shape parameters were selected as the granular materials. Direct shear tests were conducted to investigate the shear strength and the volume change responses of interfaces that generated by the interaction between surface structure with various inclination of asperities and particles with different characteristics. The testing program covers a constant $R_{max}$ of 1 mm and initial relative density ($D_r$) of 90%. For comparison, a smooth sheet with no asperity was tested to indicate the positive effects of surface topography on the mechanical behavior of the interface.

## 2. Mechanical Model

Most of the existing friction models considered the adhesion of the lubricating and dry interface which aiming at reducing device wear and extending service life (Komvopoulos et al., 1986; Bhushan and Nosonovsky, 2004; Horng et al., 2009). For particle-structure interface friction, the main research focuses on the micro-scale particle mechanical behavior while negelected the difference in the mechanical properties of graunlar materials caused by the different surfaces and particle shapes in engineering applications. It is crucial to consider the effect of asperity inclination differences on the shear behavior of granular materials with a saw-tooth surface. The saw-tooth surface can be simplified into multiple wedges, Therefore, in order to provide theoratical basis for analysis of the interface friction behaivors, a wedge friction model is introduced based on the simplified saw-tooth surface.

The model is shown in Fig. 1(a). The wedge model based on the friction theory indicates that there is a functional relationship between the horizontal force ($Q$) and the normal load ($F$) of the sliding object on the inclined plane. The functional relationship of the model is related to the friction coefficient ($\mu$) of contact surface and $\theta$. The ratio of shear stress over normal stress

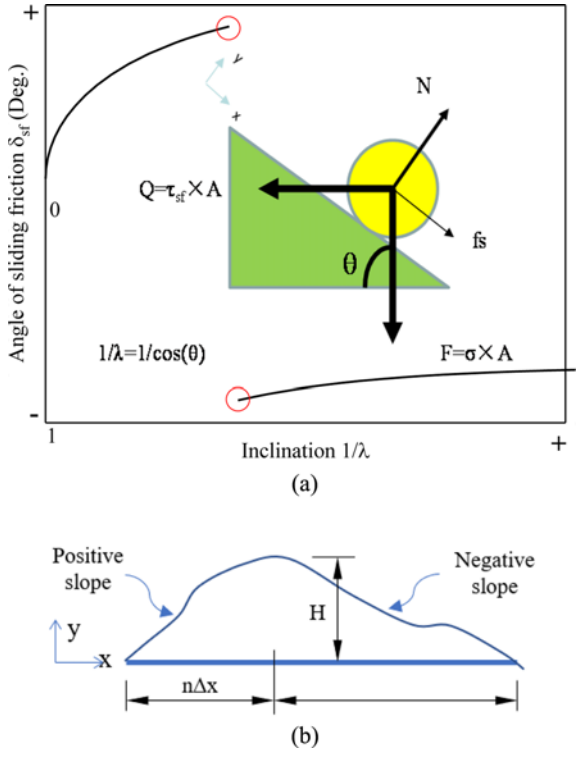


**Fig. 1.** Diagrams of Mechanical Model: (a) The Wedged Friction Model, (b) Diagram of the Definition of Interface Shape Factor

obtained by direct shear tests of various granular materials on the flat sheet surface (e.g., No. 6) is the friction coefficient between granular material and contact surface:

$$\mu = \frac{\tau_{No.6}}{\sigma}. \tag{1}$$

Then $Q$ is derived to be

$$Q \geq \frac{\sin\theta + \mu \cdot \cos\theta}{\cos\theta - \mu \cdot \sin\theta} F. \tag{2}$$

During shearing, normal load generates the normal stress on the specimen. In the same fashion, shear stress is generated by horizontal force dividing by the same contact area. Therefore, the equation is derived to be

$$\tau_{sf} \geq \frac{\sin\theta + \mu \cdot \cos\theta}{\cos\theta - \mu \cdot \sin\theta} \sigma, \tag{3}$$

where $\tau_{sf}$ is defined as the shear stress of sliding friction, and the angle of sliding friction ($\delta_{sf}$) is defined as follows:

$$\delta_{sf} = \tan^{-1}\left(\frac{\tau_{sf}}{\sigma}\right). \tag{4}$$

The evolution of $\delta_{sf}$ against inclination of asperity is depicted in Fig. 1(a). It is worth mentioning that $\delta_{sf}$ keeps going up during the early stage as the slope of inclination increases. However, when the slope of inclination reaches the critical value, $\delta_{sf}$ has become mathematically negative. The negative value indicates the wedge act as the hindrance to the object at this moment. If the sand particles slide or roll on the structure surface, the peak interface friction angle $\delta_p$, defined as the maximum mobilized interface friction angle representing the interface peak shear resistance satisfies the above wedge model.

In order to validate the reliability of the model, the interface shape factor ($\lambda$) is introduced to quantitatively describe the shape of interface. Based on the topography of saw-tooth interface that changing in only one horizontal direction, each identical asperity is divided into numerous (n) microelements and then $\lambda$ can be defined by Yi et al. (2006) as

$$\lambda = \frac{\sum_{i=1}^{n} \Delta x_i}{\sum_{i=1}^{n} \sqrt{\Delta x_i^2 + \Delta y_i^2}}, \tag{5}$$

where $\Delta x_i$ and $\Delta y_i$ are the increments of the horizontal direction and corresponding elevation direction for surface profile, respectively. the increasing direction of $\Delta x_i$ is at an obtuse angle with the direction of the interface force. Namely, it must be a positive slope in the direction of the shear force for the formula to hold (see Fig. 1(b)). For the convenient of comparison, the flat inclined plane was selected, thus, $\lambda$ can be regarded as the cosine value of the dip angle ($\theta$) of asperity in the direction of shearing.

## 3. Materials and Methods

### 3.1 Interface Materials

All the tests presented herein were performed on specimens of Ottawa sand 20/30, Dolomite sand #1, #2 and #3 and 3D printed polylactic acid (PLA) particles with different shapes. 3D printed particles with different shapes were produced via Fused Deposition Modeling (FDM) 3D printing, while sheets were produced via stereolithography (STL). Sphere (SP), Regular Octahedron (RO), Regular Hexahedron (RH) and Regular Tetrahedron (RT) were selected as four shapes of platonic solids to investigate the particle shape effects on the behavior of interface. $D_r$ of all the soil samples were prepared under a constant value of 90%. Table 1 presented physical properties of the granules for tests. It is worth mentioning that the shape was chosen to cover almost all range of the angularity in shape of the typical granular materials (Su et al., 2020). As microscopic images of granules and particle size distribution plotted in Fig. 2, all the granular materials were categorized as poorly graded sand in accordance with ASTM-2487 (2017).

After curing, the sheet had following mechanical properties: tensile strength of 60 MPa, Young's modulus of 2.9 GPa and Mons' hardness of printing sheets is from 2 to 3 which is far lower than the sands' (7). Image of printed cured sheets are also presented in Fig. 2.

### 3.2 Test Methods

Su et al. (2020) proposed shape parameter $S$ to describe a particle shape in three-dimensional based on parameter $A/V$. However, accuracy is lost in some special cases, for example when describing the shape of RH and RO. When the volume is constant, RH and RO have the same shape parameter $S$ but different mechanical characteristics. Therefore, the diameter ($L_s$) of a sphere of the same volume of the particle is utilized in accordance with Wadell (1932) with a higher accuracy and propose a new particle shape

**Table 1.** Physical Properties of Tested Soil Particles

| | Ottawa sand 20/30 | Dolomite sand | | | Printed particle | | | |
|---|---|---|---|---|---|---|---|---|
| | | 1# | 2# | 3# | SP | RO | RH | RT |
| $D_{50}$ | 0.72 | 1.40 | 0.60 | 0.30 | 2.00 | 2.00 | 2.00 | 2.00 |
| $C_u$ | 1.23 | 2.05 | 2.26 | 1.67 | 1.00 | 1.00 | 1.00 | 1.00 |
| $G_s$ | 2.650 | 2.678 | 2.678 | 2.678 | 1.24 | 1.24 | 1.24 | 1.24 |
| $e_{max}$ | 0.740 | 0.875 | 0.808 | 0.738 | 0.796 | 0.950 | 1.175 | 1.400 |
| $e_{min}$ | 0.500 | 0.483 | 0.499 | 0.509 | 0.639 | 0.715 | 0.815 | 0.867 |

Note: $D_{50}$ of printed particle in accordance with the diameter of sphere of equal volume.

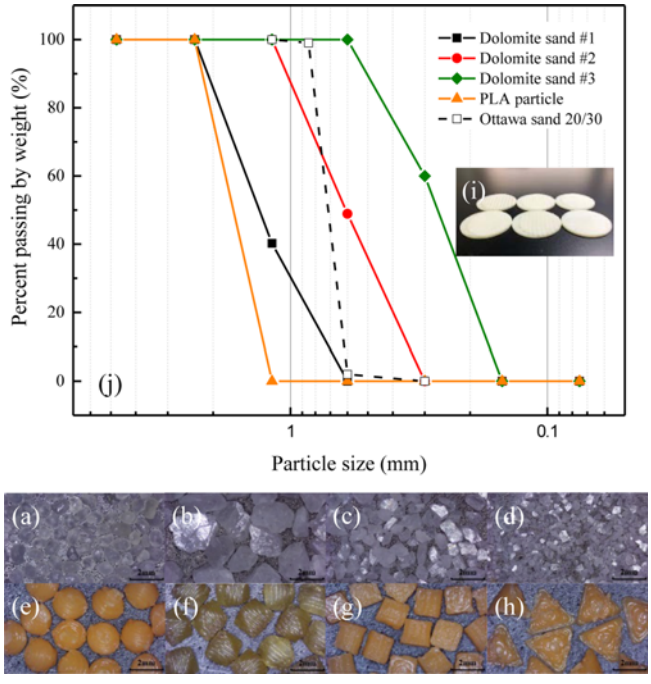


**Fig. 2.** Photographs of Test Sands and Printed Sheets: (a) Ottawa Sand 20/30, (b) Dolomite Sands 1#, (c) Dolomite Sands 2#, (d) Dolomite Sands 3#, (e) 3D Printed Plastic Particles, (f) 3D Printed Plastic Particles, (g) 3D Printed Plastic Particles, (h) 3D Printed Plastic Particles, (i) 3D Printed Sheets, (j) Particle Size Distributions of Granular Materials

parameter $S_h$ on the basis of predecessors. The $S_h$ is calculated as follows:

$$S_h = (A/V)L_s/6\,. \tag{6}$$

Note that $S_h = 1$ for SP, $S_h = 1.18$ for RO, $S_h = 1.24$ for RH and $S_h = 1.49$ for RT. For comparison, only $S_h$ is used to describe the printed particle shape.

Direct shear tests were conducted to measure the interface shear stress and the vertical displacement with the evolution of horizontal displacement. It is reported in the literature that the data obtained from direct shear tests were reliable for exploring the interface behavior (Rourke et al., 1990; Subba Rao et al., 1998). The direct shear apparatus consists of an upper and a lower cylindrical shear boxes with diameter of 61.8 mm and a displacement-controlled system.

**Table 2.** Variation of $\theta$, $\lambda$ and $1/\lambda$ of 3D Printed Sheets

| No. | Dip angle $\theta$ (Deg.) | Shape factor $\lambda$ | Inclination $1/\lambda$ |
|---|---|---|---|
| 1 | 78.6 | 0.196 | 5.10 |
| 2 | 63.4 | 0.447 | 1.41 |
| 3 | 45.0 | 0.707 | 2.24 |
| 4 | 26.6 | 0.894 | 1.12 |
| 5 | 11.4 | 0.980 | 1.02 |
| 6 | 0.00 | 1.000 | 1.00 |

Dip angle $\theta$ and $\lambda$ of asperity of the 6 printed sheets were set as shown in Table 2. The values of $\theta$ from sheet No.6 to No.1 ranged from 0 to 78.6 (degree). There is only one dip angle for one printed sheet, that means the distance between asperities and $R_{max}$ for one sheet were the same. Inclination was defined as a parameter of the reciprocal of $\lambda$. The thickness of sheet (No.6 was set 3 mm) was set to 4 mm with 1 mm for height of asperity and 3 mm for the thickness of sheet. The sheets were produced to fit inside the lower shear box frame with only asperities exposed out. The upper shear box should not be impeded during the whole shear process with 8 mm (8/61.8 = 12%) of horizontal displacement to minimize boundary effects from the shear box's sidewalls. As described by Martinez and Palumbo (2018), excessive normal stress might damage the surface of sheet printed by resin for the low hardness and thus, additional shear stress appears unexpectedly. As a result, all tests except Ottawa sand (50, 100, 200 kPa) in this investigation were performed at 50 kPa of normal stress in order to avoid the effects of surface wear/damage. At least one duplicate test was carried out and hence, a total of 120 direct shear tests were conducted on soil-structure interface which was summarized in Table 3.

## 4. Results

Because the contact area of the two cylindrical shear boxes changes during shearing, a corrected contact area must be considered in calculation of shear stress and normal stress based on the contact area corrections (Olson and Lai, 1989).

The mobilized interface friction angle $\delta_d$ and interface dilation angle $\xi$ are obtained from following equations, which exactly analogous to angles obtained in direct shear tests of granular

**Table 3.** Summary of Tests

| Test material | Type | Packing state | Particle shape | Normal stress (kPa) | Interface (No.) |
|---|---|---|---|---|---|
| Ottawa Sand | 20/30 | $Dr$ = 90% | Sub-rounded | 50, 100, 200 | 1, 2, 3, 4, 5, 6 |
| Dolomite Sand | 1# | | Angular | 50 | |
| | 2# | | | | |
| | 3# | | | | |
| Printed Particle | - | | SP | | |
| | | | RO | | |
| | | | RH | | |
| | | | RT | | |

materials (e.g., Internal friction angle $\phi$ and internal dilation angle $\psi$):

$$\delta_d = \tan^{-1}\left(\frac{\tau}{\sigma}\right), \tag{7}$$

$$\xi = \tan^{-1}\left(\frac{dv}{dh}\right), \tag{8}$$

where $\tau$ and $\sigma$ are shear and normal stresses, respectively, $dv$ and $dh$ are increments of vertical and horizontal displacement, respectively.

## 4.1 Asperity Inclination Effects on the Interface Mechanical Behaviors

Through Figs. 3(a), 3(b) and 3(c), the shear behaviors of interface between Ottawa sand 20/30 and printed sheets under the same normal stress (50 kPa) are compared. Figs. 3(d), 3(e), 3(f) and Figs. 3(g), 3(h), 3(i) show the results with all the conditions the same but under normal stresses of 100 kPa and 200 kPa, respectively. The shear stress increase with surface roughness. However, with the increase of normal stress, the positive effect of surface topography on shear stress is not obvious. It is worth mentioning that shear data show variations under relative high normal stress (e.g., 200 kPa), resulting in a challenge of distinguishing the peak shear stress. The softness of cured resin surface makes quartz particles easy to embed into the material and causing scratches on the surface. Overturning moment imposed by shear makes particles scroll intermittently in high normal stress state, resulting in the instability of shear stress

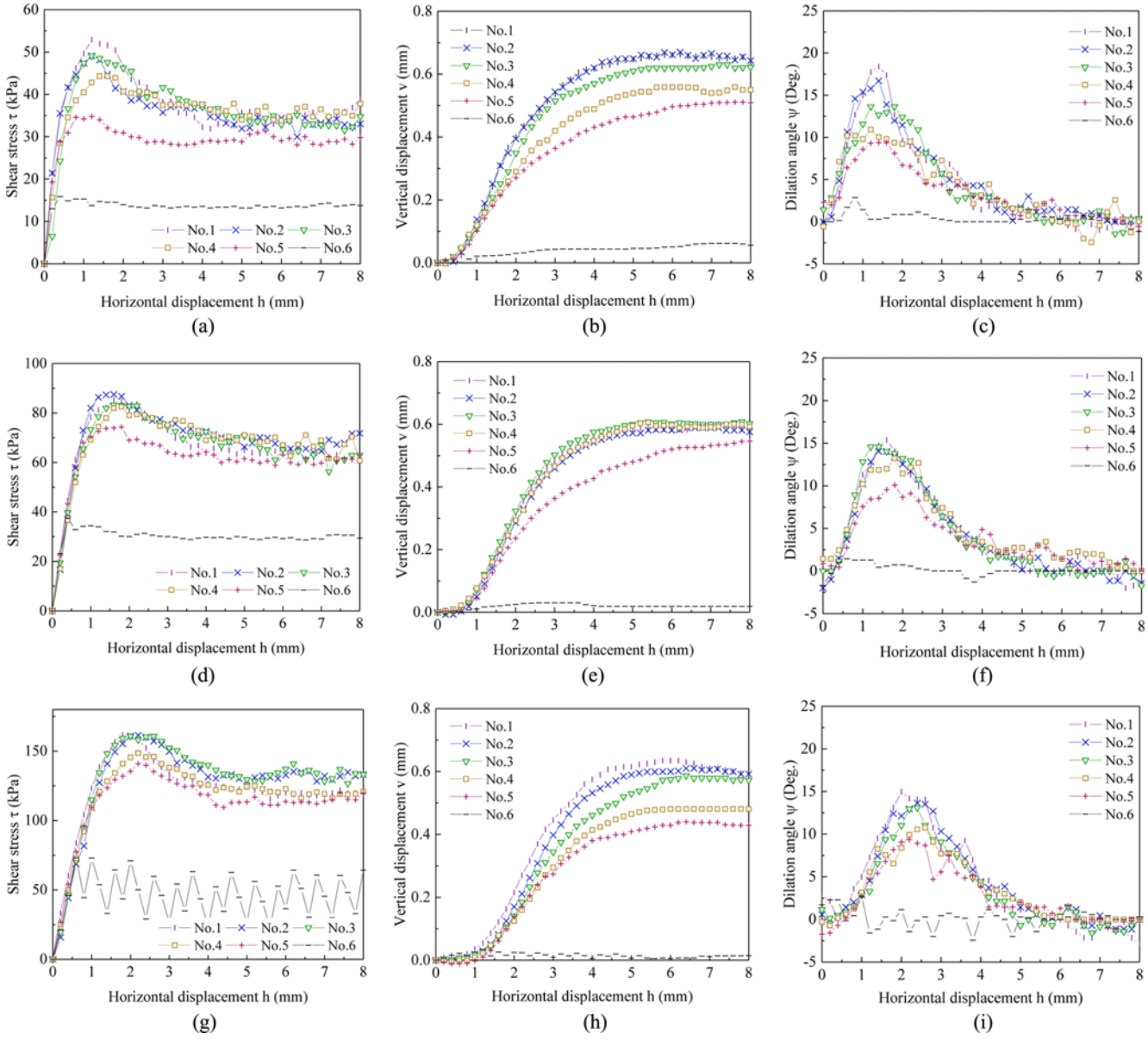


**Fig. 3.** Effects of Inclination of Asperity on Shear Stress versus Horizontal Displacement, Vertical Displacement versus Horizontal Displacement, and Dilation Angle versus Horizontal Displacement for Ottawa Sand 20/30-Printed Sheets Interfaces under Different Normal Stresses: (a, b, c) $\sigma$ = 50 kPa, (d, e, f) $\sigma$ = 100 kPa and (g, h, i) $\sigma$ = 200 kPa

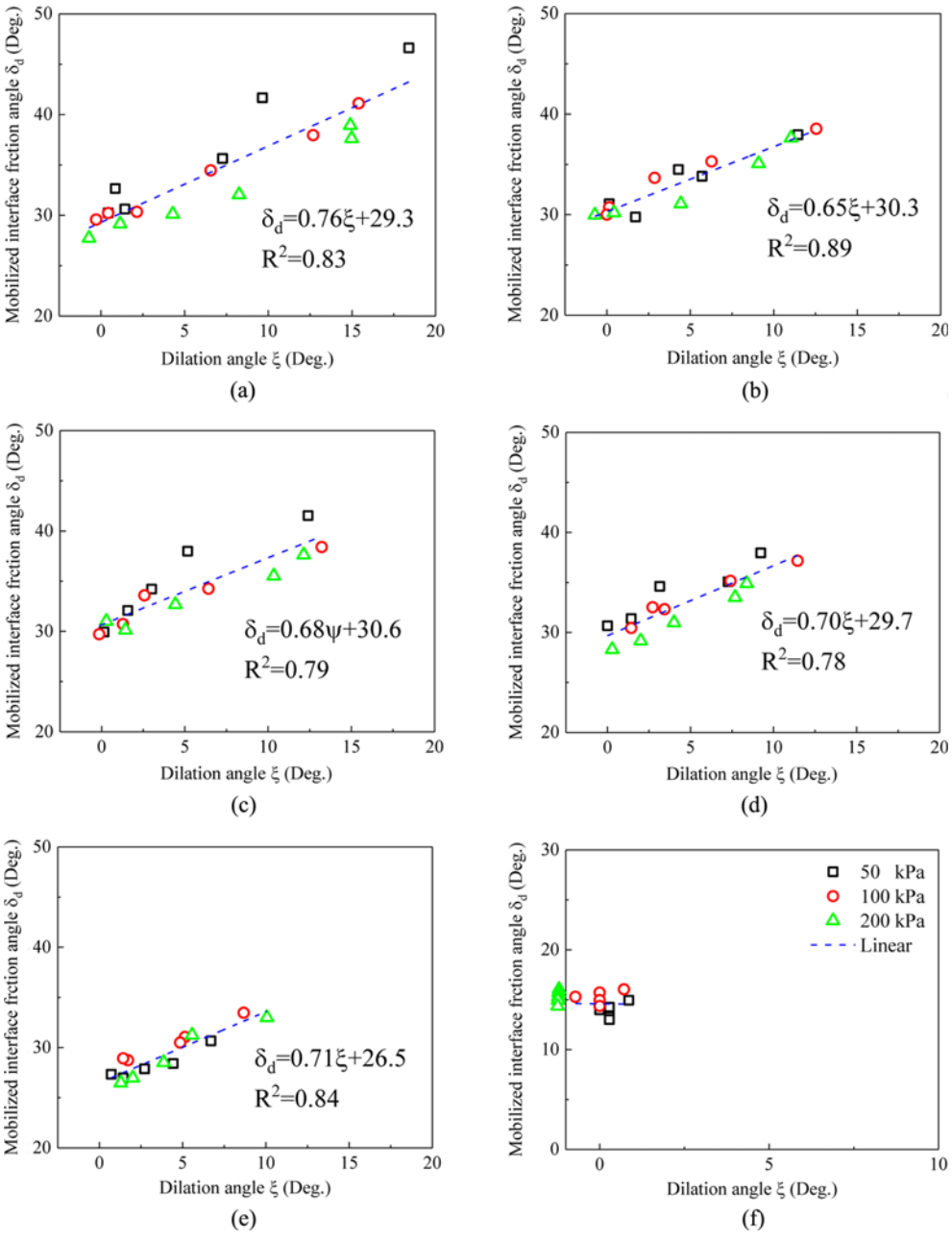


**Fig. 4.** Correlations between $\delta_d$ versus $\xi$ for Ottawa Sand 20/30-Printed Sheets Interfaces: (a) Sheet No.1, (b) Sheet No.2, (c) Sheet No.3, (d) Sheet No.4, (e) Sheet No.5, (f) Sheet No.6

(Rourke et al., 1990). In fact, only interface 6 will be affected. In other words, when the shear strength of the particles on the interface is mainly provided by the sliding of the particles, it will affect the shear behavior of the interface. Because the scratches generated by the particles on the interface only affect the movement state of the particles from sliding friction to rolling friction (Komvopoulos et al., 1986). When the shear strength of the particles on the interface is mainly provided by the rolling of the particles, it will not affect the result. When under low stress conditions, the particles will not even leave the scratches that hinders movement on the printed sheets. Therefore, the test results are reliabe.

Based on the data presented in Fig. 3, $\delta_d$ was determined and depicted in Fig. 4 against $\xi$ with the use of test data at the horizontal displacements of 2.0, 3.0, 4.0, 5.0, and 6.0 mm and at the peak state. Based on the flow rule presented by Taylor (1948), a modified version that proposed by Dietz and Lings (2006) was adapted. In consideration of the divergence in dilation angle (Bolton, 1987), a more general flow rule for interface based on Dai et al. (2016) can be written as

$$\delta_d = \varsigma \cdot \xi + \delta_{cs}, \tag{9}$$

where $\delta_{cs}$ is the interface critical state friction angle and $\varsigma$ is dilatancy coefficient. Through Figs. 4(a), 4(b), 4(c) and 4(d), we

found the intercepts are around 30 degrees for sheet No.1, 2, 3 and 4, resulting in the same postpeak state during shearing. In Fig. 4(e), the intercept is 26.5 degree for sheet No.5. The result indicates that the interface critical state of sheet No.5 is quite different from the other sheets during shearing. Therefore, the turning point of the inclination of the asperity appears between sheet No.4 and 5 (dip angle between 11.4 degree to 26.6 degree). For Fig. 4(f), it shows an evidence that a very smooth surface makes the interface dilation angle negligible resulting in the failure of establishment of relationship between $\delta_d$ and $\xi$ (Lings and Dietz, 2005).

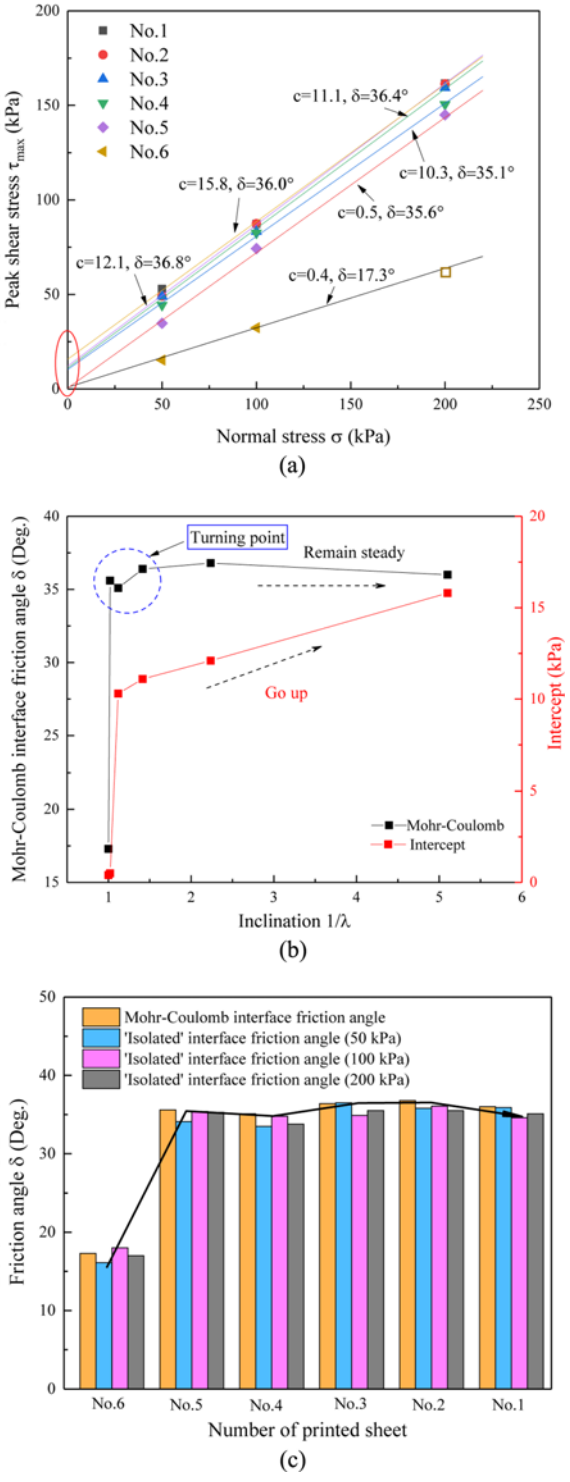


**Fig. 5.** Effects of Inclination on the Ottawa sand 20/30-Printed Sheets Interfaces: (a) Peak Shear Stress versus Normal Stress, (b) Mohr-Coulomb Interface Friction Angle and Intercept versus Inclination, (c) Friction Angle versus Number of Printed Sheet

Mohr-Coulomb shear strength envelope is plotted in Fig. 5(a). Taking the test results under 200 kPa normal stress into account, all the results are plotted in the figure while the peak interface friction angle of sheet No.6 is determined to be 17.3 degree (Rourke et al., 1990). When the inclination of asperity exceeds the "turning point", a resistance similar to 'adhesion' appears and slightly increases with the increment of inclination of surface asperity. For comparison, the intercept and slope (Mohr-Coulomb interface friction angle $\delta$) of all the Ottawa sand 20/30-printed sheets interfaces are summurized in Fig. 5(b). A turning point is shown in the figure, which governs the evolution of $\delta$, and leads to the bilinear relationship (Uesugi and Kishida, 1986a). The $\delta$ remains constant while the intercept keeps going up in the evolution of inclination of asperity. The inclination of the asperity has an effect on increasing the passive resistance from the interface topography.

Consequently, when there is no normal stress applying on the sample, the peak shear stress obtained is called the passive resistance ($P$), and the 'isolated' interface friction angle ($\delta_{if}$) (Martinez and Frost, 2017) is calculated as follows:

$$\delta_{if} = \tan^{-1}\left(\frac{\tau_{\max} - P}{\sigma}\right). \tag{10}$$

Figure 5(c) reports the evolution of $\delta_{if}$ with the increment of inclination of asperity which indicates that interface friction angle is equal to sand-sand internal friction angle without the passive resistance in this situation (Uesugi and Kishida, 1986a; Lings and Dietz, 2005; Dietz and Lings, 2006). Interparticle shear, compared with the interface shear, tends to occur in soil sample when interface friction angle approaches to the internal friction angle. In fact, the $\delta_{if}$ reflects the interparticle interactions. Interface topography is not the critical factor in determining the shear resistance of interface in this situation. Mohr-Coulomb interface friction angle can be regarded as an average value of 'isolated' interface friction angles. It is worth mentioning that when surface topography forms substantial obstacles to particles, passive resistance is not a negligible factor and thus, interface shear strength shall not be considered only by interface friction angle, and passive resistance from surface topography should also be considered.

## 4.2 Particle Size and Shape Effects on the Interface Mechanical Behaviors

Figure 6(a) reports the size effects of granular materials on interface mechanical behaviors. Dolomite sand #3 exhibits a greater shear strength than sand #2 and sand #1 when it comes to sheet No.6. Namely, interface shear resistance decreases

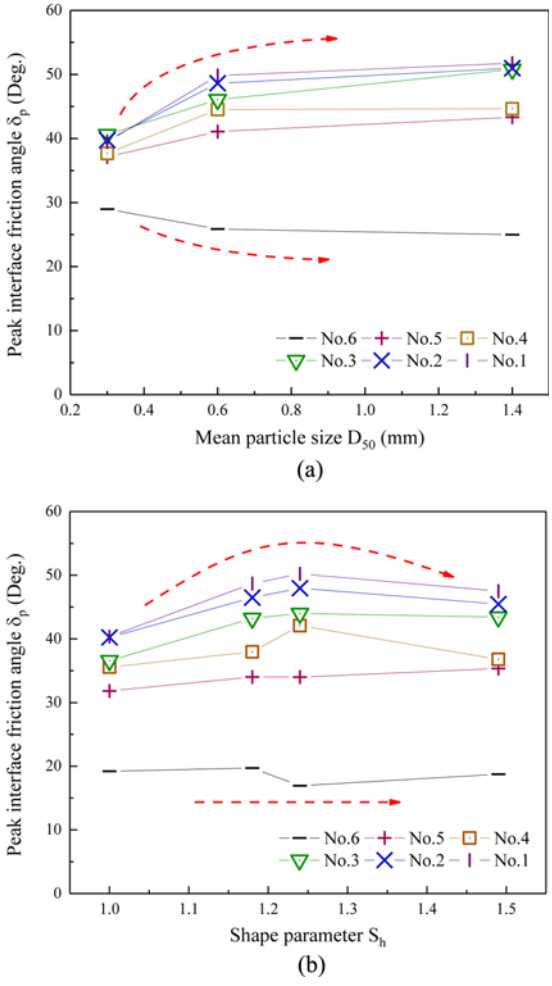


**Fig. 6.** Effects of Particle Characteristics on Peak Interface Friction Angle: (a) Effects of $D_{50}$ on Dolomite Sand-Printed Sheets Interfaces, (b) Effects of $S_h$ on PLA Particles-Printed Sheets Interfaces

with the increment of particle size. For other sheets, interface shear resistance increases with the increment of particle size. The relationship between $\delta_p$ and $D_{50}$ changes in the opposite direction with the change of the inclination of asperity. This results indicate that two different shear behaviors existing in the evolution of inclination of asperity caused by the difference in surface topography.

Figure 6(b) reports the shape effects of granular materials on interface mechanical behaviors. Particle shape affects the peak interface friction angle at the stable zone that is similarly as the effects of internal friction angle. Namely, $\delta_p$ increases at beginning then drops down with the increment of particle shape parameter $S_h$. The reasons that account for this are shown as follows:

1. The angularity of granular materials increases the probability of particle interlocking at the shear band. Particles tend to move away from the initial position and disturb other particles instead of rotating themselves that rely on friction when being sheared. 'The movemet of particles is not only in the tangential direction but also in the upward normal direction' which enhances the shear strength of interface that contacted with angular materials by governing the interparticle shear resistance (Rowe, 1962; Hryciw and Irsyam, 1993).
2. Particle shape affects the packing state of granular materials under constant relative density. The increase in $S_h$ leads to the increment in extreme void ratios, $e_{max}$ and $e_{min}$, which affects the shear resistance between interparticles (Santamarina and Cho, 2004; Cho et al., 2006; Torquato and Jiao, 2009). The angularity enhances the shear resistance. On the contrary, the increment of void ratio abates the probability of interlocking which results in the decrease in interparticle shear resistance. That explains why $\delta_p$ increases at beginning then drops down with the increment of particle shape parameter $S_h$.

The interface shear resistance governed by particle shape shows the same variation as that of the sand-sand internal shear behavior, which indicates that particle shape controls the interface shear behavior by controlling the internal shear resistance of particles at the stable zone. Namely, the shear behavior of interface is dependent on the evolution of inclination of the asperity.

## 5. Discussions

### 5.1 The Direction Dependent Interface Mechanical Behaviors

The discovery of turning point in Fig. 5 indicates that particles move on the interface have two different ways of movement (sliding and rolling). The component of shear resistance for soil-structure interfaces varies with the surface topography of the interface. According to the results in this investigation, it is found that the shear resistance of the interface can be divided into two main parts: one is the shear resistance between granular materials and saw-tooth asperity on the surface, which is named as the Bearing resistance (BR); the other is the internal shear resistance of the granular materials when particles are blocked in the gaps of asperities, which is called the Internal friction (IF). BR can be further divided into two parts based on whether particles slide along the inclined plane or not. One is the resistance from the sliding friction on the surface, which is defined as the Sliding friction (SF); the other is the resistance mobilized by the existence of asperity when particles encounter the edge of asperity on the material surface, which is defined as the Passive resistance (PR) (Frost and DeJong, 2005; Martinez and Frost, 2017).

The friction angles of Ottawa sand 20/30-printed sheet interfaces are summerized in Fig. 7(a). When $1/\lambda$ of the asperity is below the turning point, particles slide or roll along the surface, $\delta_p$ matches the trend of $\delta_{sf}$ very well. Otherwise, particles are trapped in the gaps and do not move, the behavior of interface stays at the stable zone and doesn't follow the wedge friction model. Therefore, the shear behavior of sand particles on the saw-tooth surface can be predicted by the wedge model. If the particles cannot move on the saw-tooth surface, the wedge

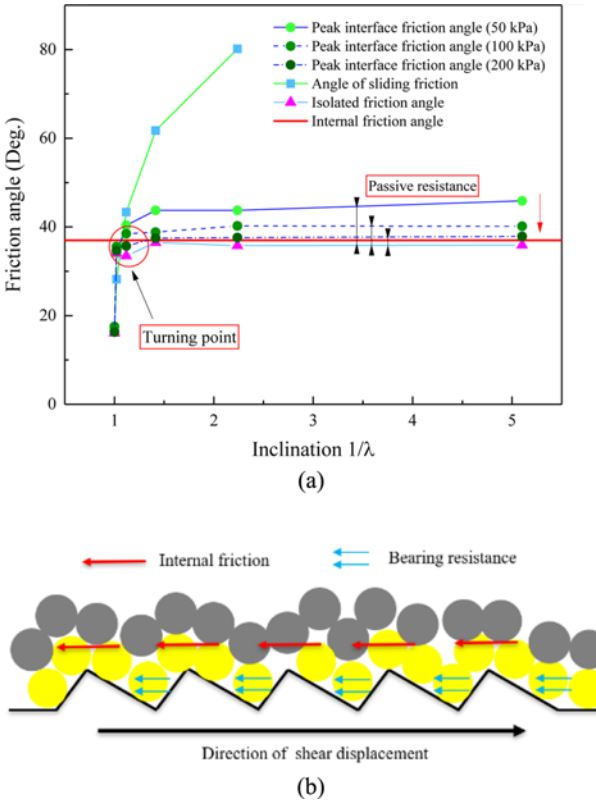


**Fig. 7.** Interpretation of the Mechanical Behaviors of Direction Dependent Interface: (a) Comparison of Friction Angles, (b) Load-Transfer Mechanism

friction model will fail and the interface shear behavior meets the laws of shear behavior interparticles, passive resistance can not be ignored. It is worth mentioning that when under high normal stresses, the $\delta_p$ is closer to $\phi$. High normal stress condition is more likely to minimize the effects of passive resistance caused by surface topography. The surface topography is no longer the dominant in affecting interface mechanical behavior. The interpretation of directional correlation of interface mechanical behavior can be drawn in Fig. 7(b).

## 5.2 Correlations between Particle Shape and Interface Mechanical Behaviors

Based on the surface microstructure image measured by atomic force microscope (AFM) plotted in Fig. 8, we found the $R_{max}$ of sheet No.6 is less than 1 μm, which is smaller than the height of asperity of saw-tooth structure. The test results on sheet No.6 are in close agreement with the findings reported by Uesugi and Kishida (1986a). The $R_n$ of surface was widely used in estimating the interface mechanical behavior (Hu and Pu, 2004; Jing et al., 2017; Martinez and Palumbo, 2018). When two adjacent peaks in the longitudinal profile can be measured in a gage length of L = $D_{50}$, the interface shear strength is inversely proportional to $D_{50}$. However, when taking $D_{50}$ as a gage length, it results in a failure in measuring two adjacent peaks in the longitudinal profile. In other words, when the size of the surface topography

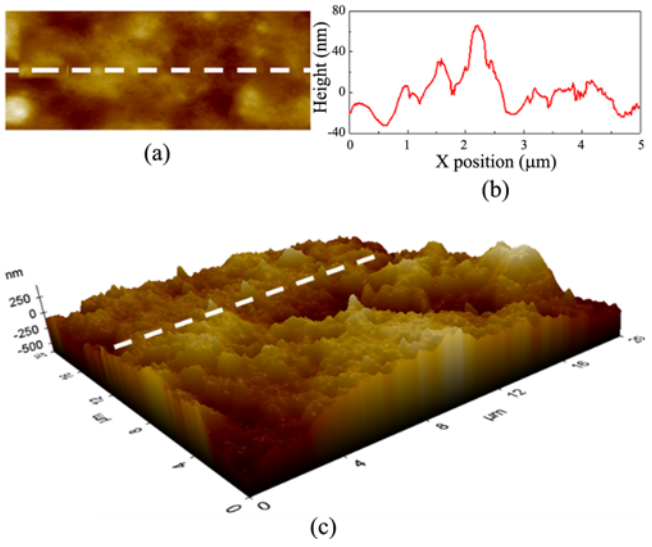


**Fig. 8.** Surface Microstructure Image of sheet No.6 by AFM: (a) 2D Topography, (b) Height of Surface Profile, (c) 3D Image of Surface

is within the same order of magnitude as $D_{50}$, the asperity becomes a substantial obstacle to the particles and thus, $D_{50}$ no longer governs the interface shear resistance by following the $R_n$ rule, however, it directly affects the internal shear resistance. It is investigated that particles with larger $D_{50}$ would exhibit greater interparticle shear resistance and thus, the $\delta_p$ is proportional to the $D_{50}$ in this zone.

The investigation of interface shear behavior using both spheres and particles with more angularity manufactured by 3D printing will provide important contributions to the understanding of the effect of particle shape on the mechanical behavior of granular materials around saw-tooth asperities. For sheet No.6, it is found that the relationship between interface shear resistance and particle shape is hard to obtain. However, RH particles exhibit minimum shear resistance when acting on smooth surface.

A relationship between the mechanical behavior of interface and the inclination of asperity governed by particle size and shape is summarized in Fig. 9. With the evolution of inclination of asperity, three different zones are divided according to the mechanical behavior of interface: (a) Zone I (smooth or almost no inclination): Soil particles slide on the sheet surface with all the shear resistance originated from SF; (b) Zone II (inclination of asperity gets larger): Shear stress increases with the increment of inclination of asperity with shear resistance resulted from SF and IF; (c) Zone III (higher inclination of asperity): When passing the turning point, soil particles are blocked in the gap of saw-tooth asperities while the shear resistance is consisted by IF and PR. IF remains constant and PR keeps growing but very slow. When granular materials slide on smooth surface, the interaction between surface and particles is dominated by sliding friction. The particles with great angularity will have higher chance of interlocking than rounded particles, and thus, internal shear resistance may not be generated easily. In other words,

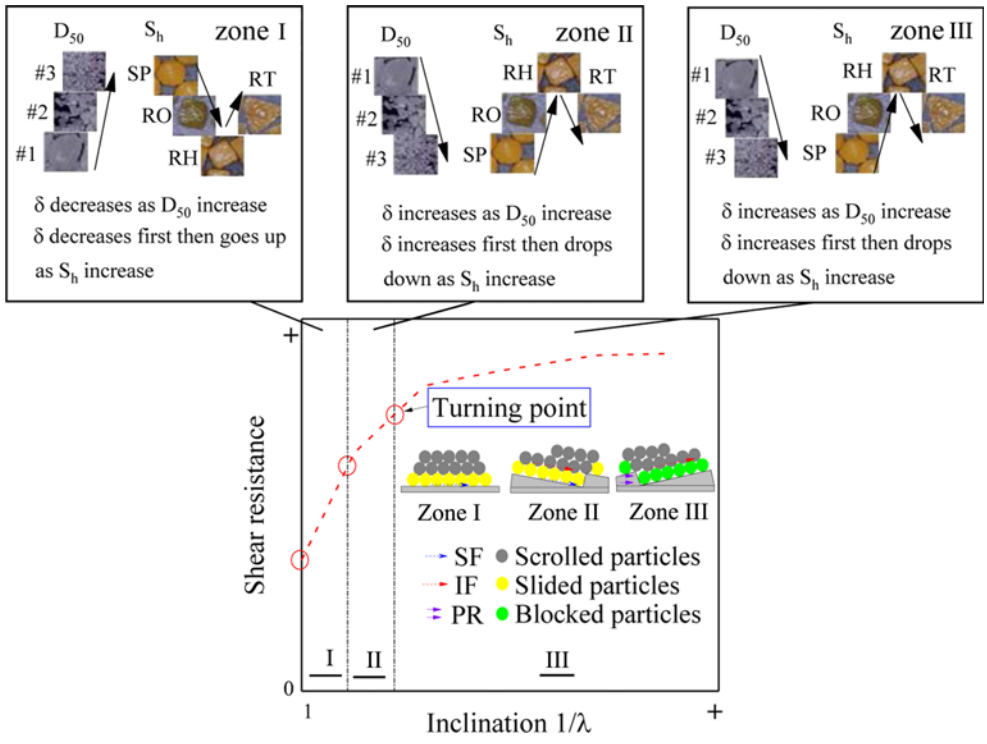


**Fig. 9.** Evolution of Shear Resistance with Different Inclination of Asperities, Particle Sizes and Shapes

round particles may increase the interface shear resistance by generating the internal shear resistance of particles. Therefore, the interface shear resistance obtained by RH particles is smaller than that obtained by SP particles and RO particles. However, in zone I, particles properties are not the dominant factors controlling the shear behaviors of the interface. When the inclination of asperity is large enough and the internal shear will not be ignored, the particle shape governs the internal shear resistance and increase the interface shear resistance of angular particles. Therefore, in zone III, the shear behavior of the interface is mostly governed by the interparticle friction.

For different asperity inclinations of the interface, the evolution of interface behavior with particle size and shape will follow the wedge friction model developed in the paper based on the laboratory investigation. However, it should be noted that the results presented above is based on low stress state, and further study on high stress level is highly desired.

## 6. Conclusions

In this research, 3D printing is employed to study the mechanical behavior of direction dependent mechanical behaviors of soil-structure interfaces through interface direct shear tests. Ottawa sand and Dolomite sand with different sizes and shapes, and six 3D printed sheets with various saw-tooth asperity inclinations were adopted to investigate the particle size and shape effects on the interface mechanical behaviors. Based on the particle movement direction on the wedge surface, this study developed a wedge friction model for predicting the interface shear behavior, and introduced the interface shape factor ($\lambda$) to quantitatively describe the roughness of the saw-tooth interface. It can be concluded that the shear resistance of interface can be divided into two main parts: Bearing resistance (BR), and Internal friction (IF). The test results indicate the positive effect of passive resistance on enhancing the shear strength of the soil-structure interface. When the inclination of asperity increases to produce passive resistance to the soil sample on the interface, the change of interface topography has little effect on the shear resistance. Particle size and shape control the interface shear resistance through changing the internal shear behavior. This finding revealing that IF is also an important part in enhancing the shear resistance and deciding the upper limit strength of interface. Finally, a bilinear relationship was observed which fully capture the interface mechanical behavior that the movement of particle on the surface changes from sliding and rolling into static blocking. In addition, three different zones that corresponding to different interface mechanical behaviors were identified with the evolution of surface asperity inclination.

## Acknowledgments

The present work was carried out with the support from the National Natural Science Foundation of China (51938005, 51808207), and High-level Talent of Innovative Research Team of Hunan Province, China (2019RS1030).

## Nomenclature

$D_{50}$ = Mean particle size
$dh$ = Increment of horizontal displacement
$D_r$ = Initial relative density
$dv$ = Increment of vertical displacement
$F$ = Normal load
$P$ = Passive resistance
$Q$ = Horizontal force
$R_{cr}$ = Critical relative roughness
$R_{max}$ = Maximum height of asperity
$R_n$ = Relative roughness
$S_h$ = Particle shape parameter
$\delta$ = Mohr-Coulomb interface friction angle
$\delta_d$ = Mobilized interface friction angle
$\delta_{if}$ = 'Isolated' interface friction angle
$\delta_p$ = Peak interface friction angle
$\delta_{sf}$ = Angle of sliding friction
$\theta$ = Dip angle of asperity
$\lambda$ = Interface shape factor
$\mu$ = Friction coefficient
$\xi$ = Interface dilation angle
$\sigma$ = Normal stress
$\varsigma$ = Dilatancy coefficient
$\tau$ = Shear stress
$\tau_{max}$ = Peak shear stress
$\tau_{sf}$ = Shear stress of sliding friction
$\phi$ = Internal friction angle
$\psi$ = Internal dilation angle

## Acknowledgments

Not Applicable

## ORCID

Xin Kang https://orcid.org/0000-0002-9758-9100
Hang Lei https://orcid.org/0000-0003-2782-0749
Renpeng Chen https://orcid.org/0000-0001-6968-4955

## References

Adamidis O, Alber S, Anastasopoulos I (2020) Assessment of three-dimensional printing of granular media for geotechnical applications. *Geotechnical Testing Journal* 43(3):20180259, DOI: 10.1520/GTJ20180259

Afzali-Nejad A, Lashkari A, Shourijeh PT (2017) Influence of particle shape on the shear strength and dilation of sand-woven geotextile interfaces. *Geotextiles and Geomembranes* 45(1):54-66, DOI: 10.1016/j.geotexmem.2016.07.005

ASTM D2487 (2017) Standard practice for classification of soils for engineering purposes (unified soil classification system). ASTM D2487, ASTM International, West Conshohocken, PA, USA

Bhushan B, Nosonovsky M (2004) Comprehensive model for scale effects in friction due to adhesion and two- and three-body deformation (plowing). *Acta Materialia* 52:2461-2474, DOI: 10.1016/j.actamat.2004.01.038

Bolton MD (1987) Discussion: The strength and dilatancy of sands. *Géotechnique* 37(2):219-226, DOI: 10.1680/geot.1987.37.2.219

Cho GC, Dodds J, Santamarina JC (2006) Particle shape effects on packing density, stiffness, and strength: Natural and crushed sands. *Journal of Geotechnical and Geoenvironmental Engineering* 132(5):591-602, DOI: 10.1061/(ASCE)1090-0241(2006)132:5(591)

Dai BB, Yang J, Zhou CY (2016) Observed effects of interparticle friction and particle size on shear behavior of granular materials. *International Journal of Geomechanics* 16(1):04015011, DOI: 10.1061/(ASCE)GM.1943-5622.0000520

DeJong JT, Burrall M, Wilson DW, Frost JD (2017) A bio-inspired perspective for geotechnical engineering innovation. Geotechnical Frontiers 2017 No. 862-870, American Society of Civil Engineers, Reston, VA, USA

Dietz MS, Lings ML (2006) Postpeak strength of interfaces in a stress-dilatancy framework. *Journal of Geotechnical and Geoenvironmental Engineering* 132(11):1474-1484, DOI: 10.1061/(ASCE)1090-0241(2006)132:11(1474)

Dove JE, Jarrett JB (2002) Behavior of dilative sand interfaces in a geotribology framework. *Journal of Geotechnical and Geoenvironmental Engineering* 128(1):25-37, DOI: 10.1061/(ASCE)1090-0241(2002)128:1(25)

Farhadi B, Lashkari A (2017) Influence of soil inherent anisotropy on behavior of crushed sand-steel interfaces. *Soils and Foundations* 57(1):111-125, DOI: 10.1016/j.sandf.2017.01.008

Frost JD, DeJong JT (2005) In situ assessment of role of surface roughness on interface response. *Journal of Geotechnical and Geoenvironmental Engineering* 131(4):498-511, DOI: 10.1061/(ASCE)1090-0241(2005)131:4(498)

Hanaor DAH, Gan Y, Revay M, Airey DW, Einav I (2016) 3D printable geomaterials. *Géotechnique* 66(4):323-332, DOI: 10.1680/jgeot.15.P.034

Horng JH, Wei CC, Tsai HJ, Shiu BC (2009) A study of surface friction and particle friction between rough surfaces. *Wear* 267:1257-1263, DOI: 10.1016/j.wear.2009.02.017

Hryciw RD, Irsyam M (1993) Behavior of sand particles around rigid ribbed inclusions during shear. *Soils and Foundations* 33(3):1-13, DOI: 10.3208/sandf1972.33.3_1

Hu L, Pu J (2004) Testing and modeling of soil-structure interface. *Journal of Geotechnical and Geoenvironmental Engineering* 130(8):851-860, DOI: 10.1061/(ASCE)1090-0241(2004)130:8(851)

Jardine RJ, Lehane BM, Everton SJ (1993) Friction coefficients for piles in sands and silts. Springer, Berlin, Germany, 661-677

Jing XY, Zhou WH, Li Y (2017) Interface direct shearing behavior between soil and saw-tooth surfaces by DEM simulation. *Procedia Engineering* 175:36-42, DOI: 10.1016/j.proeng.2017.01.011

Kang X, Cambio D, Ge L (2012) Effect of parallel gradations on crushed-rock concrete interface behaviors. *Journal of Testing and Evaluation* 40(1):1-8, DOI: 10.1520/JTE103773

Kang X, Ge L, Chang KT, Kwok AO (2016) Strain-controlled cyclic simple shear tests on sand with radial strain measurements. *Journal of Materials in Civil Engineering* 28(4):0405169, DOI: 10.1061/(ASCE)MT.1943-5533.0001458

Kang X, Kang GC (2015) Modified monotonic simple shear tests on silica sand. *Marine Georesources and Geotechnology* 33(2):122-126, DOI: 10.1080/1064119x.2013.805289

Komvopoulos K, Saka N, Suh NP (1986) Plowing friction in dry and lubricated metal sliding. *Journal of Tribology* 108:301-312, DOI:

10.1115/1.3261181
Lee SJ, Lee CH, Shin M, Bhattacharya S, Su YF (2019) Influence of coarse aggregate angularity on the mechanical performance of cement-based materials. *Construction and Building Materials* 204:184-192, DOI: 10.1016/j.conbuildmat.2019.01.135
Lings ML, Dietz MS (2005) The peak strength of sand-steel interfaces and the role of dilation. *Soils and Foundations* 45(6):1-14, DOI: 10.3208/sandf.45.1
Liu CN, Ho YH, Huang JW (2009) Large scale direct shear tests of soil/PET-yarn geogrid interfaces. *Geotextiles and Geomambranes* 27:19-30, DOI: 10.1016/j.geotexmem.2008.03.002
Martinez A, Frost JD (2017) The influence of surface roughness form on the strength of sand-structure interfaces. *Géotechnique Letters* 7(1):1-8, DOI: 10.1680/jgele.16.00169
Martinez A, Palumbo S (2018) Anisotropic shear behavior of soil-structure interfaces: Bio-inspiration from snake skin. IFCEE 2018 No. 94-104, American Society of Civil Engineers, Reston, VA, USA
Michalowski RL, Čermák J (2002) Strength anisotropy of fiber-reinforced sand. *Computers and Geotechnics* 29:279-299, DOI: 10.1016/S0266-352X(01)00032-5
Milligan GWE, Tei K (1998) The pull-out resistance of model soil nails. *Soils and Foundations* 38(2):179-190, DOI: 10.3208/sandf.38.2_179
Mitchell JK, Villet WCB (1987) Reinforcement of earth slopes and embankment. National Cooperative Highway Research Program Report No.290, Washington DC, USA
Olson RE, Lai JR (1989) Direct shear testing. Advanced Geotechnical Laboratory, Dept. of Construction Engineering, Chaoyang University of Technology, Taichung, Taiwan, ROC
Portelinha FHM, Zornberg JG, Pimentel V (2014) Field performance of retaining walls reinforced with woven and nonwoven geotextiles. *Geosynthetics International* 21(4):270-284, DOI: 10.1680/gein.14.00014
Rourke BTDO, Druschel SJ, Netravali AN (1990) Shear strength characteristics of sand-polymer interfaces. *Journal of Geotechnical Engineering* 116(3)451-469, DOI: 10.1061/(ASCE)0733-9410(1990)116:3(451)
Rowe PW (1962) The stress-dilatancy relation for static equilibrium of an assembly of particles in contact. *Proceedings of the Royal Society A* 269(1339):500-527, DOI: 10.1098/rspa.1962.0193
Santamarina JC, Cho GC (2004) Soil behaviour: The role of particle shape. Advances in geotechnical engineering: The Skempton conference: Proceedings of a three day conference on advances in geotechnical engineering, March 29-31, London, UK
Su YF, Bhattacharya S, Lee SJ, Lee CH, Shin M (2020) A new interpretation of three-dimensional particle geometry: M-A-V-L. *Transportation Geotechnics* 23:100328, DOI: 10.1016/j.trgeo.2020.100328
Subba Rao KS, Rao KSS, Allam MM, Robinson RG (1998) Interfacial friction between sands and solid surfaces. *Proceedings of the institution of civil engineers. Geotechnical Engineering* 131(2):75-82, DOI: 10.1680/igeng.1998.30112
Sukumaran B, Ashmawy AK (2001) Quantitative characterisation of the geometry of discret particles. *Géotechnique* 51(7)619-627, DOI: 10.1680/geot.2001.51.7.619
Tang CS, Shi B, Zhao LZ (2010) Interfacial shear strength of fiber reinforced soil. *Geotextiles and Geomembranes* 28(1):54-62, DOI: 10.1016/j.geotexmem.2009.10.001
Taylar DW (1948) Fundamentals of soil mechanics. John Wiley, New York, NY, USA
Tehrani FS, Han F, Salgado R, Prezzi M, Tovar RD, Castro AG (2016) Effect of surface roughness on the shaft resistance of non-displacement piles embedded in sand. *Géotechnique* 66(5):386-400, DOI: 10.1680/jgeot.15.P.007
Tiwari B, Ajmera B, Kaya G (2010) Shear strength reduction at soil structure interface. GeoFlorida 2010, February 20-24, Orlando, FL, USA, DOI: 10.1061/41095(365)177
Torquato S, Jiao Y (2009) Dense packings of the Platonic and Archimedean solids. *Nature* 460(7257):876-879, DOI: 10.1038/nature08239
Uesugi M, Kishida H (1986a) Frictional resistance at yield between dry sand and mild steel. *Soils and Foundations* 26(4):139-149, DOI: 10.3208/sandf1972.26.4_139
Uesugi M, Kishida H (1986b) Influential factors of friction between steel and dry sands. *Soils and Foundations* 26(2):33-46, DOI: 10.3208/sandf1972.26.2_33
Wadell H (1932) Volume, shape, and roundness of rock particles. *The Journal of Geology* 40(5):443-451
Wang J, Dove JE, Gutierrez MS (2007) Anisotropy-based failure criterion for interphase systems. *Journal of Geotechnical and Geoenvironmental Engineering* 133(5):599-608, DOI: 10.1061/(ASCE)1090-0241(2007)133:5(599)
Won MS, Kim YS (2007) Internal deformation behavior of geosynthetic-reinforced soil walls. *Geotextiles and Geomembranes* 25(1):10-22, DOI: 10.1016/j.geotexmem.2006.10.001
Yavari N, Tang AM, Pereira JM, Hassen G (2016) Effect of temperature on the shear strength of soils and the soil–structure interface. *Canadian Geotechnical Journal* 53(7):1186-1194, DOI: 10.1139/cgj-2015-0355
Yi C, Wang CJ, Zhang L, Chen ZH, Xie HP (2006) Study on description index system of rough surface based on bi-body interaction (in Chinese). *Chinese Journal of Rock Mechanics and Engineering* 25(12):2481-2492
Yudhbir, Abedinzadeh R (1991) Quantification of particle shape and angularity using the image analyzer. *Geotechnical Testing Journal* 14(3):296, DOI: 10.1520/GTJ10574J